SIXTH EUROPEAN ROTORCRAFT AND POWERED LIFT AIRCRAFT FORUM

Paper No. 70

A SIMPLE SYSTEM FOR HELICOPTER INDIVIDUAL-BLADE-CONTROL AND ITS APPLICATION TO GUST ALLEVIATION

Norman D. Ham
Robert M. McKillip, Jr.
Massachusetts Institute of Technology
Cambridge, Mass., U.S.A.

September 16-19, 1980

Bristol, England

THE UNIVERSITY, BRISTOL BS81HR, ENGLAND

A SIMPLE SYSTEM FOR HELICOPTER INDIVIDUAL-BLADE-CONTROL AND ITS APPLICATION TO GUST ALLEVIATION

Norman D. Ham*

Robert M. McKillip, Jr.**
Department of Aeronautics and Astronautics
Massachusetts Institute of Technology
Cambridge, Massachusetts 02139

Abstract

A new, advanced type of active control for helicopters and its application to gust alleviation is described. Each blade is individually controlled in the rotating frame over a wide range of frequencies up to the sixth harmonic of rotor speed. Considerable system simplification is achieved by means of modal decomposition.

It is shown both analytically and experimentally that by utilizing a tip-mounted accelerometer as a sensor in the feedback path, significant reductions in blade flapping response to a sinusoidal gust can be achieved at the gust excitation frequency as well as at super- and subharmonics of rotor speed.

1. Introduction

A truly advanced helicopter rotor must operate in a severe aerodynamic environment with high reliability and low maintenance requirements. This environment includes:

(1) atmospheric turbulence (leading to impaired flying qualities, particularly in the case of hingeless rotor helicopters).

(2) blade-vortex interaction in transitional and nap-of-the-earth flight (leading to unacceptable higher harmonic blade bending stresses and helicopter vibration).

(3) retreating blade stall flutter (leading to large torsional loads in blade structure and control system).

(4) blade-fuselage interference (leading to unacceptable higher harmonic blade bending stresses and helicopter vibration).

(5) blade instabilities due to flap-lag coupling, high advance ratio (including blade "sailing" during shut-down), and high advancing blade Mach number.

(6) blade aerodynamic and/or mass mismatch due to battle or other damage (leading to large one-per-rev vibration and possible loss of control). This is an extreme example of the common blade out-of-track problem.

The application of feedback techniques make it possible to alleviate the effects described in items (1) to (6) above, while improving helicopter vibration and handling characteristics to meet desired standards. The concept of Individual-Blade-Control (IBC) embodies the control of broadband electrohydraulic actuators attached to the swash plate or individually to each blade, using signals from sensors mounted on the blades to supply appropriate control commands to the actuators[1,2]. Note that the IBC involves not just control of each blade independently, but also a feedback loop for each blade in the rotating frame. In this manner it becomes possible to reduce the severe effects of atmospheric turbulence, blade-vortex interaction, retreating blade dynamic stall, blade-fuselage interference, blade instabilities, and blade mismatch, while providing improved flying qualities. Blade automatic tracking capability may also be achieved, and it may even be possible to eliminate the conventional swash plate.

2. Description of the IBC System

The severe dynamic environment of the helicopter rotor includes atmospheric turbulence, vibration, dynamic stall, blade instabilities, and blade imbalance as described in the Introduction. The excitation frequencies of these rotor blade disturbances cover a broad band, roughly from 1 Hz to 30 Hz in a medium-sized helicopter. Such frequencies require an actuator response time of .003 seconds, which is currently achievable[1]. Figure 1 presents the frequency band required by the IBC system. It is seen that there is a low frequency domain from 0 to 1Ω involving helicopter gust response, flying qualities, blade instabilities, and ground resonance, and a high frequency domain from 1Ω to 6Ω involving blade bending stress, vibration and stall flutter.

Also shown in Figure 1 are the frequencies of the blade modes likely to be affected. Low frequency effects will primarily affect the blade flapping mode, which has a natural frequency near unity. Blade high advance ratio instability occurs at 0.5Ω or 1Ω and also involves the blade flapping mode[3]. Blade flap-lag instability couples the flapping mode and the first blade inplane mode which has a natural frequency of about 0.3Ω (hinged blade), 0.7Ω ("soft" inplane hingeless blade) or about 1.2Ω ("stiff" inplane hingeless blade). Pilot's control of the blade flapping mode occurs at 1Ω, and it is essential that the IBC system does not degrade control effectiveness. Higher harmonic vibration will primarily affect the blade flatwise bending mode, having a natural frequency near 3Ω, and possibly the blade first torsion mode which has a natural frequency around 5Ω, and finally, blade stall flutter involves the blade first torsion mode.

It is evident that the IBC system will be most effective if it is comprised of several subsystems, each controlling a specific mode, e.g., the blade flapping mode, the first blade inplane

This research was sponsored by the Ames Research Center, NASA, Moffett Field, California 94035. Major contributions to the project were made by P.H. Bauer and C. Cholaj.

*Director, VTOL Technology Laboratory
**Research Engineer.

mode, the first blade flatwise bending mode, and the first blade torsion mode. Each sub-system operates in its appropriate frequency band, and extraneous sensor signal frequencies are excluded by appropriate filtering.

The feedback signals for the IBC system will be provided by blade-mounted accelerometers, capable of sensing blade flatwise, inplane, and torsional accelerations. For example, in Figure 2, the flatwise acceleration at r = R for the case of the blade flapping mode is given by

$$a_F \simeq (R-e)\ddot{\beta} + R\,\Omega^2\beta$$

and for any sinusoidal variation of flap angle of amplitude $\bar{\beta}$ and frequency ω,

$$a_F = [1-(\omega/\Omega)^2(1-e/R)]\,\Omega^2\bar{\beta}\,\sin\omega t$$

This signal will be strongly frequency-dependent, producing a value proportional to blade flapping angle at low frequencies ($\omega << \Omega$) and one proportional to flapping acceleration at high frequencies ($\omega >> \Omega$), while having a negligible output at frequencies close to rotational frequency, i.e., the pilot's control frequency. This behavior further assists in the development of multiple feedback paths that appropriately filter the accelerometer signal and utilize different compensation networks for the various portions of this signal in order to achieve desired blade modal response over the full frequency spectrum.

As discussed above, the four most significant modes of blade motion are:

(1) blade flapping mode (or first flatwise bending mode for a hingeless blade)

(2) blade first inplane mode (pinned or cantilever)

(3) blade first flatwise bending mode (or second for a hingeless blade)

(4) blade first torsion mode (including control flexibility)

Modal decomposition is accomplished by frequency placement, frequency filtering, and accelerometer orientation. Control of each of the above modes will now be discussed as separate IBC sub-systems of the type shown in Figure 3.

The blade flapping mode dominates low frequency effects such as gust response and flying qualities. It is also the means by which the pilot achieves desired helicopter control moments. Finally, blade flapping instability occurs at 0.5/rev. or 1.0/rev. in the rotating coordinate system of Figure 1[3].

In the terminology of Figure 3, for the flapping mode IBC sub-system the filter would be designed to eliminate flatwise accelerometer signals above one/rev., i.e. those due to the high frequency modes, and the loop compensation would be selected to optimize the sub-system in the frequency range from zero to one/rev. The desired filter characteristics would be augmented by the zero accelerometer signal near one/rev. The flatwise accelerometer ideally would not sense blade motion in the first inplane mode, thus eliminating inputs due to motion in this mode. This sub-system acts somewhat as a frequency-dependent δ_3-hinge without the undesirable side effects of deterioration of autorotative or powered landing flare capability, or amplification of higher harmonic vibration. In addition, modal damping can be increased either by appropriate choice of compensation, or by means of inter-blade coupling[4].

The blade first inplane mode dominates instabilities of the so-called ground or air resonance type. In the terminology of Figure 3, for the first inplane mode sub-system, the filter would be designed to eliminate inplane accelerometer signals above or below the modal frequency, and the loop compensation would be selected to achieve the level of modal damping necessary for stability.

The blade first flatwise bending mode (or second for a hingeless blade) dominates helicopter higher harmonic blade bending stresses and vibration due to its near-resonance with the 3/rev. airloading on the blade. In the flatwise bending mode sub-system, the filter would be designed to eliminate flatwise accelerometer signals above and below 3/rev., i.e., those due to blade flapping and second blade flatwise bending displacements, and the loop compensation would be selected to optimize the sub-system at 3/rev. In addition, the desired filter characteristics could be augmented by a zero accelerometer signal near one/rev. which would be obtained by appropriate spanwise location of the accelerometer.

The blade first torsion mode dominates the high frequency blade torsional dynamic instability known as stall flutter, which occurs at a frequency close to the blade torsion mode frequency[5]. In the torsion mode sub-system, the filter would be designed to eliminate signals from the accelerometers (oriented to sense torsional motion only) above and below the blade torsion mode frequency, and the loop compensation would be selected to achieve the level of modal damping necessary for stability. Since a large portion of the blade is unstalled during stall flutter, potential flow aerodynamics can be used to estimate the pitch damping moment generated by this portion of the oscillating blade to offset the negative pitch damping of the stalled portion.

The configuration shown in Figure 3 employs an individual actuator and multiple feedback loops to control each blade. These actuators and feedback loops rotate with the blades and, therefore, a conventional swash plate is not required. However, actuator reliability considerations may outweigh the simplicity of this configuration. In this case, the same degree of individual-blade-control can be achieved by placing the actuators in the non-rotation system and controlling the blades through a conventional swash plate. The actual configuration then depends upon the number of blades:

No. of Blades	Collective	Differential Collective	Longitudinal Cyclic	Lateral Cyclic
2	X	X		
3	X		X	X
4	X	X	X	X

Note that individual-blade-control can thus be achieved in the non-rotating system if the number of control degrees-of-freedom equals the number of blades.

For more than three blades, the use of extensible blade pitch control rods in the form of hydraulic actuators is a possibility.

3. Theoretical Analysis

Given the articulated offset-hinged rotor blade shown in Figure 2, the flapping equation of motion is obtained by summing moments about the offset hinge:

$$\int_e^R [(r-e)^2\ddot{\beta} + r(r-e)\Omega^2\beta]dm = \int_e^R (r-e)\,dL \qquad (1)$$

where for $\psi = \Omega t$,

$$dL = \frac{1}{2}\rho ac[\theta U_T^2 - U_P U_T]dr$$

$$U_T = \Omega r + \mu\Omega R \sin\psi$$

$$U_P = \lambda\Omega R + (r-e)\dot{\beta} + \mu\Omega R\beta\cos\psi$$

and defining

$$x = \frac{r}{R},$$

$$\xi = \frac{e}{R}$$

$$I_1 = \int_e^R (r-e)^2 dm, \quad \text{the blade flapping inertia}$$

$$\gamma = \frac{\rho acR^4}{I_1}, \quad \text{the Lock number}$$

substitution into equation 1 yields, after some algebra:

$$\frac{\ddot{\beta}}{\Omega^2} + [A+H\mu\sin\psi]\frac{\dot{\beta}}{\Omega} + [1+G+C\mu\cos\psi + \frac{1}{2}\mu^2 E\sin 2\psi]\beta$$

$$= \theta[B + \frac{1}{2}\mu^2 E + 2C\mu\sin\psi - \frac{1}{2}\mu^2 E\cos 2\psi]$$

$$- [C\lambda + E\lambda\mu\sin\psi] \qquad (2)$$

where

$$A = \frac{\gamma}{2}(\frac{1}{4} - \frac{2}{3}\xi + \frac{1}{2}\xi^2 - \frac{1}{12}\xi^4)$$

$$B = \frac{\gamma}{2}(\frac{1}{4} - \frac{1}{3}\xi + \frac{1}{12}\xi^4)$$

$$C = \frac{\gamma}{2}(\frac{1}{3} - \frac{1}{2}\xi + \frac{1}{6}\xi^3)$$

$$E = \frac{\gamma}{2}(\frac{1}{2} - \xi + \frac{1}{2}\xi^2)$$

$$G = \frac{1}{I_1}\int_e^R e(r-e)\,dm$$

$$H = \frac{\gamma}{2}(\frac{1}{3} - \xi + \xi^2 - \frac{1}{3}\xi^3)$$

$$I = \int_e^R (r-e)^2 dm$$

In addition to the pitch excitation terms on the right hand side of equation 2, one must add the forcing terms due to the gust distribution across the rotor disk[6]:

$$\frac{\gamma}{2}\int_\xi^1 x^2 w_G dx + \frac{\gamma}{2}\mu\sin(\Omega t)\int_\xi^1 x w_G dx$$

where

$$w_G = \bar{w}_G \sin(\omega t - \phi_G)$$

$\bar{w}_G$ = gust amplitude/rotor tip speed, ΩR

$$\phi_G = 2\pi\frac{Rx\cos(\Omega t)}{\lambda_G} = \frac{1}{\mu}(\frac{\omega}{\Omega})x\cos(\Omega t)$$

and substitution of this gives the following expression for the nondimensional gust excitation:

$$w_G = \bar{w}_G[\sin\omega t\cos\phi_G - \cos\omega t\sin\phi_G]$$

Evaluation of the two integrals after series expansion of $\cos\phi_G$ and $\sin\phi_G$ then yields the following terms:

$$\bar{w}_G\sin\omega t\,\{\frac{\gamma}{6}(1-\xi^3) - \frac{\gamma}{40}\frac{1}{\mu^2}(\frac{\omega}{\Omega})^2(1-\xi^5) + \frac{\gamma}{896}\frac{1}{\mu^4}(\frac{\omega}{\Omega})^4(1-\xi^7)\}$$

$$+\bar{w}_G\cos(\Omega-\omega)t\{\frac{\gamma}{8}\mu(1-\xi^3) - \frac{\gamma}{16}\frac{1}{\mu}(\frac{\omega}{\Omega})(1-\xi^4) - \frac{3\gamma}{128}\frac{1}{\mu}(\frac{\omega}{\Omega})^2(1-\xi^4)$$

$$+ \frac{\gamma}{192}\frac{1}{\mu^3}(\frac{\omega}{\Omega})^3(1-\xi^6) + \frac{\gamma}{3072}\frac{1}{\mu^3}(\frac{\omega}{\Omega})^4(1-\xi^6)$$

$$- \frac{\gamma}{6144}\frac{1}{\mu^5}(\frac{\omega}{\Omega})^5(1-\xi^8)\}$$

$$+\bar{w}_G\cos(\Omega+\omega)t\{-\frac{\gamma}{8}\mu(1-\xi^2) - \frac{\gamma}{16}\frac{1}{\mu}(\frac{\omega}{\Omega})(1-\xi^4) + \frac{3\gamma}{128}\frac{1}{\mu}(\frac{\omega}{\Omega})^2 x$$

$$(1-\xi^4) + \frac{\gamma}{192}\frac{1}{\mu^3}(\frac{\omega}{\Omega})^3(1-\xi^6) - \frac{\gamma}{3072}\frac{1}{\mu^3}(\frac{\omega}{\Omega})^4(1-\xi^6)$$

$$- \frac{\gamma}{6144}\frac{1}{\mu^5}(\frac{\omega}{\Omega})^5(1-\xi^8)\} + \text{H.O.T.}$$

These are then added to the RHS of equation 2 to describe the rigid flapping response to pitch and

gust inputs. This expression contains periodic coefficients that can be eliminated using the harmonic balance technique as described below.

Standard harmonic balance solutions involve a simple substitution of assumed harmonic motion expressions, and then an equating of coefficients of like periodic functions. These assumed motions included a steady-state term plus harmonics at the gust excitation frequency (ω), rotor rotation frequency (Ω), and at the first subharmonic ($\Omega-\omega$) and superharmonic ($\Omega+\omega$) of the rotation frequency:

Flapping motion:

$$\beta(t) = \beta_o + \bar{\beta}_c \cos \omega t + \bar{\beta}_s \sin \omega t + \hat{\beta}_c \cos \Omega t + \hat{\beta}_s \sin \Omega t + \beta'_c \cos(\Omega-\omega)t + \beta'_s \sin(\Omega-\omega)t + \beta''_c \cos(\Omega+\omega)t + \beta''_s \sin(\Omega+\omega)t$$

Pitching motion:

$$\theta(t) = \theta_o + \bar{\theta}_c \cos \omega t + \bar{\theta}_s \sin \omega t + \hat{\theta}_c \cos \Omega t + \hat{\theta}_s \sin \Omega t + \theta'_c \cos(\Omega-\omega)t + \theta'_s \sin(\Omega-\omega)t + \theta''_c \cos(\Omega+\omega)t + \theta''_s \sin(\Omega+\omega)t$$

Substitution of these expressions into equation 2 resulted in a matrix equation relating the nine blade flapping coefficients to the gust and pitch excitation terms. This matrix equation was then solved to extract the flapping coefficients[7].

4. Model Design and Construction

The rotor test facility shown in Fig. 4 was developed for the research described in Ref. 6. For simplicity and ease of modification it was decided to equip a single rotor blade with electro-mechanical pitch control, counter balanced by two "dummy" blades of 5/8 inch steel drill rod and adjustable counterweights. Geometric restrictions were imposed upon the hardware, however, to make it possible to add two more identical but separate pitch actuators without redesign.

The blade used in the test rotor was the same as that of Reference 6, having a NACA 0012 section with a 21.2-inch span and two-inch chord. It had an eight degree linearly decreasing twist from root to tip and was constructed of fiberglass with aluminum reinforcing. The blade was connected to the rotor hub by means of a ball-and-socket root fixture permitting flapping, lagging and feathering degrees of freedom about the same point. A complete set of rotor parameters can be found in Table 1.

The individual-blade control assembly consisted of a shaft-mounted servo motor that, through a series of linkages, acted as a position controller of the rotor blade pitch angle. The motor/tachometer was mounted between two 1/4-inch-thick disks of aluminum, which also held two counterweights to offset the inertia contribution of the motor. These disks were fixed to the shaft by two aluminum blocks containing two setscrews and a keyway. Also, attached to the forward disk was an aluminum support for the transmission shaft of the control assembly.

This transmission shaft was mounted at a right angle to the motor shaft, and was given its rotation by a spiral-bevel gear that was driven by a pinion on the motor shaft, with a 2:1 gear reduction ratio. This same shaft was attached to a thin aluminum bar that had a threaded rod inserted through its other end, and parallel to the transmission shaft. Mounted on the threaded rod was yet another actuator link that consisted of two rod ends screwed together by a threaded metal coupling. The other end of the link was connected to a bolt that passes through the blade pitch axis.

The rotor blade was rigidly attached to a steel fork assembly that, in turn, bolted to the inner race of a spherical bearing. The spherical bearing was then contained within a steel support block that was clamped fast to the main rotor hub, thus allowing fully articulated blade motion with concentric pitch, flap and lead-lag axes, offset from the hub by approximately two inches. The blade root fixture was instrumented with strain gauges mounted on a .005-inch-thick curved steel flexure that was free to turn about the lead-lag axis, but gave a torsional output corresponding to blade flapping, and a bending output corresponding to blade pitch angle. This particular flexure geometry was chosen as a solution to the problem of uncoupling the three rigid degrees of freedom of the blade for purposes of measurement. A thickness of .005 inches was selected for the flexure to produce a significant signal for small blade deflections, while at the same time providing negligible resistance to the blade flapping motion.

Since the servo motor was to function as a position control device, it was necessary to incorporate appropriately weighted feedback signals to the motor amplifier. These signals were the motor speed, taken from the tachometer, and the angular position, measured from the torsional strain gage mounted on the steel fixture attached to the blade. A block diagram of the control system can be seen in Figure 5. Both of these signals were used as feedback to achieve a faster system response for the same stability level. Further details are given in Ref. 7.

5. Design of the Gust Alleviation System

In order to have some guidelines for approaching the problem of synthesis of a gust alleviation system design, an adequate definition of the requirements for the system response was necessary. Since primary helicopter control is achieved through orientation of the rotor thrust vector with respect to the fuselage, it is obvious that tighter control over orientation of the tip path plane (and hence the thrust vector) will improve the vehicle's handling qualities. In the rotating frame these pilot commands are either very low frequency (with respect to rotor rotation) such as thrust and maneuvering commands, or at rotor

rotational speed, relating to static positioning of the tip path plane in space. Hence, any blade flapping due to an external disturbance, such as a low frequency gust, can be viewed as a perturbation to be attenuated as quickly as possible. A block diagram of the IBC system can be seen in Figure 6.

Since the work described here was performed upon a model rotor, the task of tracking a simulated pilot command was secondary to reducing the effects of a gust disturbance upon the forward flight flapping response of the blade. The emphasis in the design process was directed at low-frequency flap attenuation, while producing no ill-effects upon the high-frequency flapping response, and with the simplest configuration possible.

Design of the IBC rotor system was complicated by the presence of periodic terms in the blade's equation of motion, as can be seen in Section 3. These trigonometric terms, however, are first or second order in μ (advance ratio), and thus drop out in the case of hovering flight. Because of this phenomenon, a constant coefficient approximation for the blade flapping equation is possible over the range of low advance ratios. As a check to see if this approximation was valid for the model rotor used in the experiments, Floquet analysis was applied to equation 2, and the poles of the blade characteristic equation were found not to vary significantly for $\mu < 0.7$.

The decision was then made to use classical control theory to design the gust-alleviation system, with evaluation of the design to be made using the harmonic balance technique described above. Though this initial approach seemed adequate, closed-loop tests of an early feedback design were found to produce half-per-revolution oscillations in the flapping response at $\mu = 0.4$. Further investigation using Floquet theory showed that such a response could be predicted analytically, and henceforth all proposed IBC designs were checked for such phenomena using this method.

In order to understand the effects of each of the dynamic components present in the IBC system, it becomes necessary to consider each block of Figure 6 separately. If it were possible to sense blade flapping angle directly, and if we had an ideal pitch servo, the simplest IBC system would be a pure gain feedback or in effect, an electronic data-three hinge. The effect of such a design can be seen in a root-locus plot. As the gain is increased, the blade pole moves vertically away from the real axis, thus decreasing its damping. The corresponding Bode plot shows that as the gain is increased, the low frequency response is decreased at the expense of increased flapping response at frequencies above rotor rotational. It should be emphasized again at this point that the behavior suggested by such classical control analysis assumes a single input, single output constant coefficient system, an assumption only valid in hovering flight. Hence, even though the frequency response indicated by the Bode plot suggests that the superharmonic flapping response (arising due to forward flight) should be amplified, one cannot be certain of the actual response until the harmonic balance approach is applied to the feedback design.

Although the IBC model described here is instrumented (via a flexure and strain gauge mounted at the blade root fitting) to measure flap angle directly, it was felt that a more desirable means to provide such a signal to the feedback path, one that could be realized on a full-scale machine, was the use of a blade-tip-mounted accelerometer as the sensing element.

Such an orientation contributes a complex conjugate pair of zeroes, located directly on the imaginary axis. Thus, as one increases the static sensitivity of this blade/accelerometer system, the blade pole moves directly over to this complex zero, reducing its damping while not significantly changing its natural frequency. The corresponding Bode plot shows that because of the accelerometer's amplification of blade flapping accelerations at frequencies above rotor rotation, it appears possible to attenuate high-frequency flapping perturbations as well as low-frequency disturbances.

But these two designs are unrealistic since they do not consider the effects of pitch-actuator dynamics. Like any physically realizable servo system, these dynamics are essentially low-pass, in that there is attenuation of high-frequency inputs. Thus, because this actuation system is located in the feedback path of Figure 6, high frequency flapping perturbations will not be affected by the IBC system since the feedback path is essentially "broken" at the servo block. The challenge, then, is to configure the actuator to have a break frequency significantly larger than rotor rotational speed.

Subsequent studies evaluated the effect of varying the actuator's inner-loop gain upon the overall response of the IBC system. As the inner-loop gain is increased, the damping of the servo's complex conjugate poles decreases, and the flapping attenuation improves. This improvement was not significant for gains beyond that of Figure 7, and thus the system of Figure 7 was selected as the final gust-alleviation system. The frequency and damping of the elements of the selected system are given in Figure 6.

Further details of the system design are given in Reference 7.

6. Testing of the Gust Alleviation System

The Wright Brothers Wind Tunnel at M.I.T. was used for IBC rotor gust alleviation testing. The test section is a 7' x 10' oval, and for rotor testing the turntable is equipped with two trunnions for horizontal mounting of the rotor shaft. This particular orientation was chosen to permit use of the existing gust generator[8].

Mounted outside of the test section was a hydraulic motor and slip-ring assembly, providing shaft rotation and data transmission from the rotating frame to the analog computer in the fixed frame. Clamped to the far trunnion was another slip-ring assembly that transmitted electrical current to the servo-motor and tachometer.

The rotor shaft was secured to the support bearings with the rotor plane in the center of the tunnel section. Instrumentation consisted of a

difference amplifier, for the amplification of blade flapping and feathering strain gage signals; a portable analog computer and servo amplifier, for processing the feedback loop signals and supplying the motor driving signal; a dual-beam storage oscilloscope, for monitoring the flap and pitch signals; a spectrum analyzer, for on-line analysis of the blade flapping response; an X-Y plotter, for the production of a hard record of the analyzer output; another oscilloscope for quick visualization of the output of the spectrum analyzer; a difference amplifier for the amplification of the accelerometer signals; a hot-wire probe and amplifier, for measurement of the gust amplitude; and finally, a PDP-11 computer, for analog-to-digital data acquisition and real-time Fast Fourier Transform Analysis. A schematic of the instrumentation layout is shown in Figure 8.

In the wind tunnel test, the parameters varied were gust excitation frequency, tunnel speed, and feedback gain (see Table 1). A typical time history of the gust, flapping, pitch, and accelerometer signals for the $\mu = 0.4$ case can be seen in Figure 9, and the spectral decomposition of this run is shown in Figure 10. The information from the spectral analyses of the gust signal was then used as input to produce the solid theoretical curves of Figure 11. Several Fast Fourier Transform analyses were performed over different segments of data for the open loop cases of the test, and the standard deviation for these data was used to construct the error bars about the data points.

The data for the various cases tested appears to match the theory reasonably well, and the correlation appears to improve with increasing advance ratio. The explanation for this trend may well be the reduction in harmonic inflow effects due to an increase in total rotor inflow.

Figure 12 shows the effect of increasing open-loop static sensitivity S_{OL} upon the IBC gust alleviation system performance. It was originally thought that possible harmonic wake effects on the model blade flapping response to pitch input would dramatically lower the feedback gain so that the expected system performance would not be realized; as can be seen in the figure, reductions at the excitation frequency are close to those predicted analytically. For low excitation frequencies, these can be rapidly calculated by considering the block diagram of Figure 6. Since the forward path between the flapping due to disturbance and the flapping output of the IBC system is unity, all gain, or static sensitivity, must appear between the output and the summing junction. Then, we have the following relation for closed-loop static sensitivity:

$$S_{CL} = \frac{1}{1 + S_{OL}}$$

and hence for open-loop static sensitivity values of 0, 0.4, 0.8 and 1.2, we obtain closed-loop static sensitivity values of 1, 0.71, 0.56 and 0.45 respectively. This number subtracted from unity gives the fractional reduction in flapping response to be expected from that particular system.

7. Application to Full Size Rotors

The Lock number of the model blade was 3.0. For a full size rotor, the increase in damping due to the increase in Lock number results in the flapping at excitation frequency becoming the dominant response[6]. Also, with increased blade damping it becomes possible to use higher feedback gain for the same stability level, and as a consequence the IBC system performance improves with increasing Lock number.

The effective Lock number can be increased on a given multi-blade rotor by inter-blade coupling. Following Ref. 4, the pitch of the blade at azimuth angle ψ is made proportional to the flapping angle of the immediately preceding blade at azimuth angle $\psi + \Delta\psi$ as follows:

$$\theta(\psi) = -K\beta(\psi + \Delta\psi)$$

Then if $\beta(\psi) = \bar{\beta} \sin\omega t$

$$\beta(\psi + \Delta\psi) = \bar{\beta} \sin \frac{\omega}{\Omega} (\psi + \Delta\psi)$$

$$= \beta(\psi) \cos \frac{\omega}{\Omega} \Delta\psi + \frac{\dot{\beta}(\psi)}{\Omega} \frac{\Omega}{\omega} \sin \frac{\omega}{\Omega} \Delta\psi$$

and the left-hand side of equation 2 becomes

$$\frac{\ddot{\beta}}{\Omega^2} + [A+(B + \frac{1}{2} E\mu^2)K_2 + \mu(H+2CK_2)\sin \Omega t$$

$$- \frac{1}{2} E\mu^2 K_2 \cos 2\Omega t] \frac{\dot{\beta}}{\Omega}$$

$$+ [1+G+(B + \frac{1}{2} E\mu^2)K_1 + \mu 2CK_1 \sin\Omega t + \mu C \cos\Omega t$$

$$+ \frac{1}{2} E\mu^2 \sin 2\Omega t - \frac{1}{2} E\mu^2 K_1 \cos 2\Omega t]\beta$$

where $K_1 = K \cos \frac{\omega}{\Omega} \Delta\psi$

$$K_2 = K \frac{\Omega}{\omega} \sin \frac{\omega}{\Omega} \Delta\psi$$

The inter-blade coupling parameters were selected as follows. For a three-bladed rotor ($\Delta\psi = 120°$) of Lock number 8.0, an open-loop static sensitivity of 1.5 was chosen as a baseline sixty-percent gust-alleviation design. Then, using the constant coefficient approximation to the flapping equation of motion, a tradeoff study was performed between the coupling parameter K and the open-loop static sensitivity while maintaining the same damping ratio of the closed-loop blade poles as that of the baseline design. For values of K beyond 1.0 it was found that the corresponding increases in static sensitivity did not produce significant improvement in gust alleviation, and thus a value of $K = 1$ was chosen. Figure 13 shows the associated root-locus and Bode plots for the three-bladed rotor with $S_{OL} = 4.0$. This gain value yields a closed loop static sensitivity of 0.20, which corresponds to a reduction in the flapping gust response of approximately 80%. This response is plotted in Figure 14 (solid line) along with the open-loop and baseline IBC designs.

Another low-frequency application of the IBC system is rotor stabilization. As shown in the

Appendix, blade flapping due to low frequency vehicle pitching, rolling, horizontal and vertical disturbances can also be alleviated by the same IBC system used for gust alleviation.[2] This implies that a helicopter with nearly neutral angle-of-attack stability and speed stability can be achieved using the IBC system.

8. Conclusions

Comparison between theory and experiment indicates that the theory of this paper is satisfactory for the purposes of IBC gust alleviation system design.

The use of an accelerometer as blade motion sensor is shown not only to be feasible, but to have unique advantages in the IBC system.

The experimental results show that substantial alleviation of rotor blade response to gusts is possible, as much as eighty percent for a full size blade with inter-blade coupling.

Since low-frequency rotor blade excitation due to helicopter pitching, rolling, horizontal or vertical disturbances is similar in nature to low-frequency gust disturbances, the IBC gust alleviation system will tend to stabilize the rotor as a whole, giving it nearly neutral angle-of-attack and speed stability.

Successful application of the IBC system to gust alleviation has motivated subsequent application of the system to blade vibration-alleviation investigations.

References

1. Kretz, M., "Research in Multicyclic and Active Control of Rotary Wings", Vertica, 1, 2, 1976.

2. Ham, N.D., "A Simple System for Helicopter Individual-Blade-Control Using Modal Decomposition", Vertica, 4, 1, 1980.

3. Biggers, J.C., "Some Approximations to the Flapping Stability of Helicopter Rotors", J.A.H.S., 19, 4, October 1974.

4. Sissingh, G.J., "Variation of Rotor Dynamic Response by Self-Contained Mechanical Feedback", IAS Paper No. 61-25, January 1961.

5. Ham, N.D. and Young, M.I., "Torsional Oscillation of Helicopter Blades Due to Stall", J. Aircraft, 3, 3, May-June 1966.

6. Yasue, M., Vehlow, C.A. and Ham, N.D., "Gust Response and Its Alleviation for a Hingeless Helicopter Rotor in Cruising Flight", Proc. Fourth European Rotorcraft Forum, Stresa, Italy, September 1978.

7. McKillip, R.M. Jr., "The Design, Testing, and Evaluation of the M.I.T. Individual-Blade-Control System as Applied to Gust Alleviation for Helicopters", M.I.T. Aeroelastic and Structures Research Laboratory TR-196-1, February 1980.

8. Ham, N.D., Bauer, P.H. and Lawrence, T.H., "Wind Tunnel Generation of Sinusoidal Lateral and Longitudinal Gusts by Circulation Control of Twin Parallel Airfoils", NASA CR-137547, August 1974.

Table 1

ROTOR TEST PARAMETERS

Number of blades	1
Radius, R	2.031 ft
Chord, c	2 in
Lock number, γ	3.01
Solidity, σ	0.0231
Collective Pitch, θ_o	8 deg
Shaft tilt angle in cruising flight, α_s	10 deg forward
Lift-curve slope, a	5.73
Rotational speed, Ω	53 rad/sec
Built-in blade angle of twist	8 deg (linear)
Feathering axis	25% chord
Hinge offset	2 in
Tunnel velocity, V	15 and 30 mph
Advance ratio, μ	0.2 and 0.4
Gust frequency $\frac{\omega}{\Omega}$	0.1 to 0.5

APPENDIX

APPLICATION OF IBC TO ROTOR STABILIZATION

The flapping equation of motion in rotating coordinates for a blade with zero hinge offset is

$$\frac{\ddot{\beta}}{\Omega^2} + \frac{\gamma}{8}\left[1 + \frac{4}{3}\mu\sin\psi\right]\frac{\dot{\beta}}{\Omega} + \left[1 + \frac{\gamma}{6}\mu\cos\psi + \frac{\gamma}{8}\mu^2\sin 2\psi\right]\beta$$

$$= \frac{\gamma}{8}\left[\left(1 + \mu^2\right) + \frac{\theta}{3}\mu\sin\psi - \mu^2\cos 2\psi\right]\theta - \frac{\gamma}{6}\left[1 + \frac{3}{2}\mu\sin\psi\right]\Delta\lambda$$

where the incremental inflow $\Delta\lambda$ includes such effects as gusts, rotorcraft vertical disturbances, and blade-vortex/blade-fuselage interaction.

Blade pitch angle θ with respect to inertial space is

$$\theta = \theta_o + \left(\theta_{1_c} - \phi\right)\cos\psi + \left(\theta_{1_s} - \alpha\right)\sin\psi$$

where α and ϕ are rotorcraft pitch and roll angles.

For the special case of a gust or vertical disturbance, $\Delta\lambda = \lambda_G + \delta$ and the equation becomes

$$\frac{\ddot{\beta}}{\Omega^2} + \frac{\gamma}{8}\left[\ \right]\frac{\dot{\beta}}{\Omega} + \left[\ \right]\beta = \frac{\gamma}{8}\left\{\theta_o\left(1 + \mu^2\right) + \frac{4}{3}\mu\left(\theta_{1_s} - \alpha\right)\right\}$$
$$+ \frac{\gamma}{8}\left\{\left(\theta_{1_c} - \phi\right)\left(1 + \frac{1}{4}\mu^2\right)\right\}\cos\psi$$
$$+ \frac{\gamma}{8}\left\{\left(\frac{\theta}{3}\mu\theta_o + \left(\theta_{1_s} - \alpha\right)\left(1 + \frac{3}{2}\mu^2\right)\right\}\sin\psi\right.$$
$$- \frac{\gamma}{6}\left(\lambda_G + \delta\right)$$
$$- \frac{\gamma}{4}\mu\left(\lambda_G + \delta\right)\sin\psi$$

neglecting harmonics above the first. It is seen that low frequency pitching (α), rolling (ϕ), horizontal (μ), gust (λ_G), and vertical (δ) disturbances can be alleviated by the same IBC system. Attenuation of the response to pilot's control would be prevented by biasing the feedback signal by a signal proportional to stick displacement.

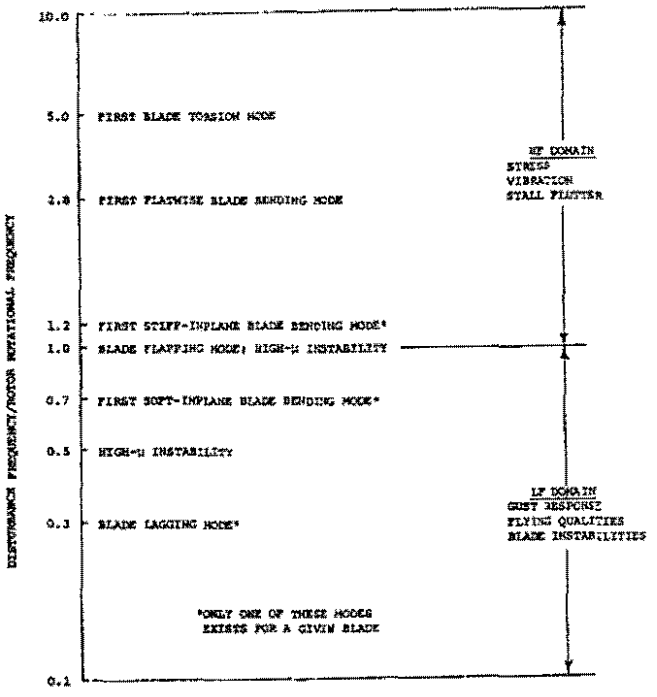

FIG. 1 FREQUENCY DOMAINS OF THE INDIVIDUAL-BLADE-CONTROL SYSTEM IN ROTATING COORDINATES

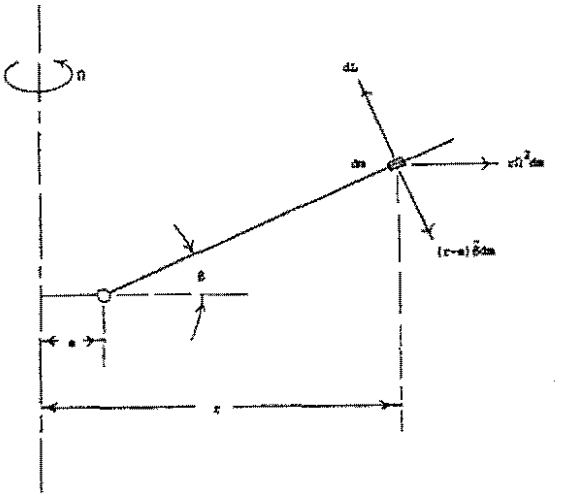

FIG. 2 BLADE ELEMENT FORCE SCHEMATIC

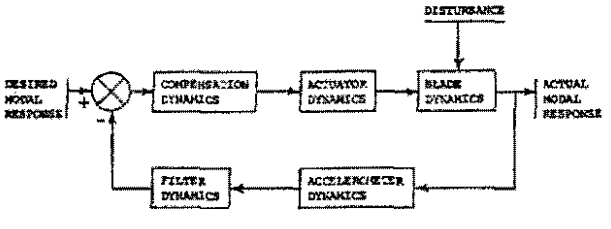

FIG. 3 INDIVIDUAL-BLADE-CONTROL SUB-SYSTEM

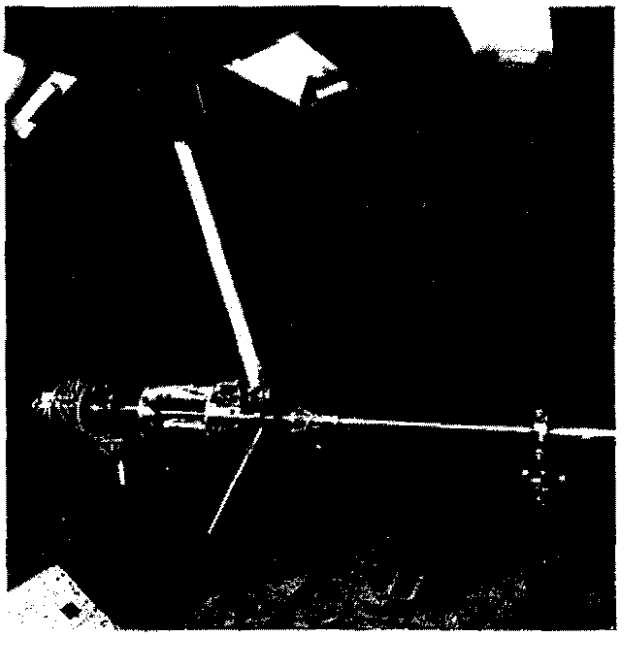

FIG. 4 INDIVIDUAL-BLADE-CONTROL ROTOR TEST FACILITY, WRIGHT BROTHERS WIND TUNNEL, MIT

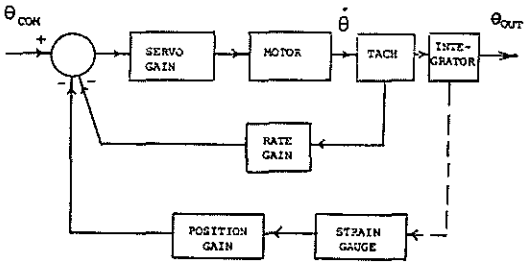

FIG. 5 SERVO SYSTEM BLOCK DIAGRAM

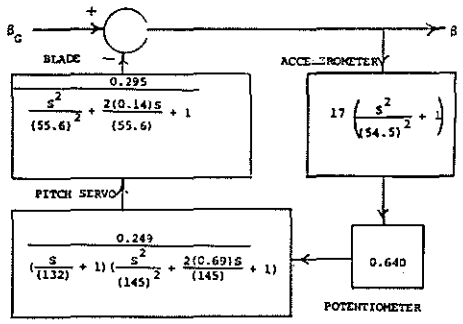

FIG. 6 GUST ALLEVIATION SYSTEM MATHEMATICAL BLOCK DIAGRAM

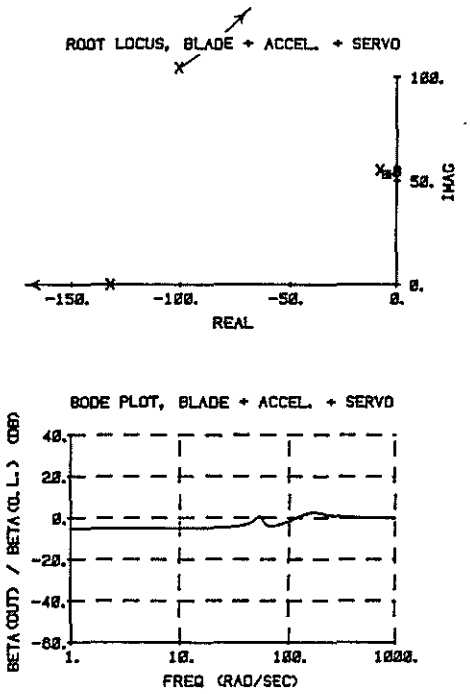

FIG. 7 BLADE, ACCELEROMETER, AND MEDIUM-GAIN-SERVO DESIGN

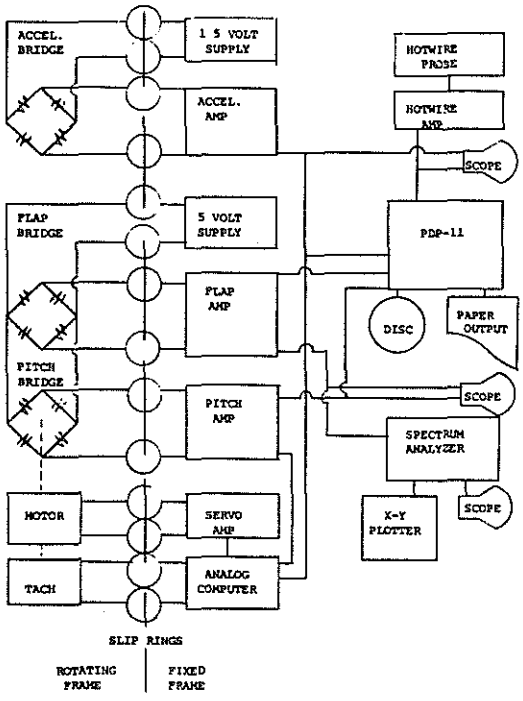

FIG. 8 INSTRUMENTATION FLOWCHART FOR WIND TUNNEL TESTS

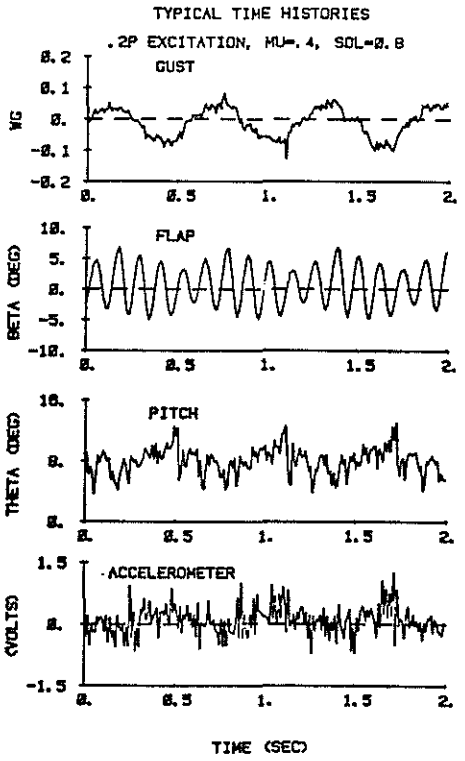

FIG. 9 TYPICAL I.B.C. GUST SYSTEM TIME HISTORY

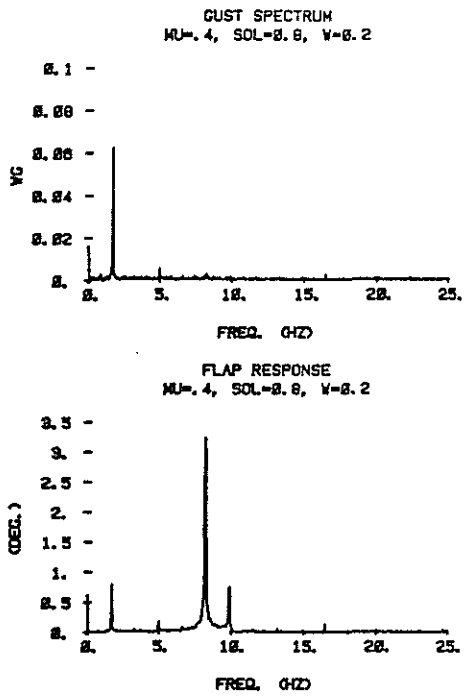

FIG. 10a SPECTRAL DECOMPOSITION OF GUST, FLAP, PITCH AND ACCELEROMETER DATA

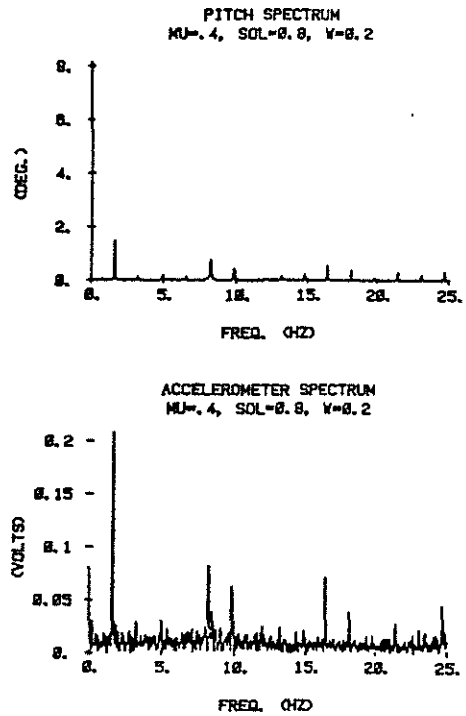

FIG. 10b (CONCLUDED)

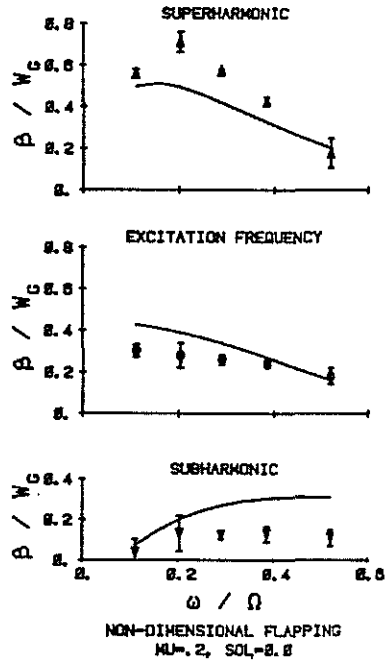

FIG. 11a NON-DIMENSIONALIZED FLAP RESPONSE TO GUST

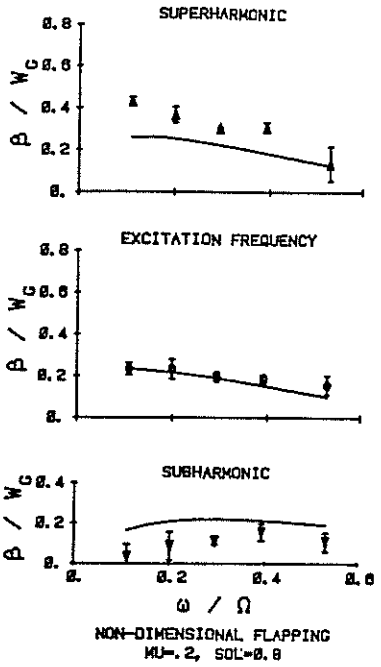

FIG. 11b (CONTINUED)

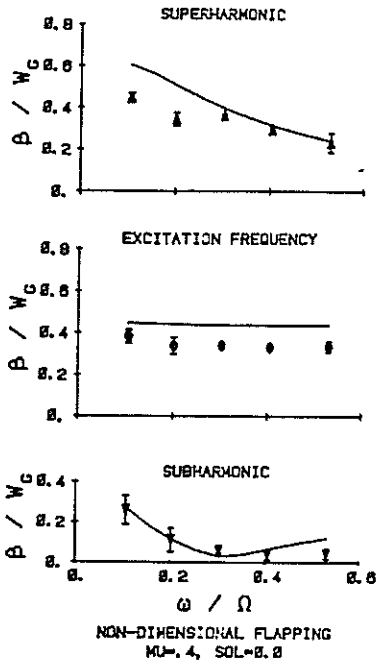

FIG. 11c (CONTINUED)

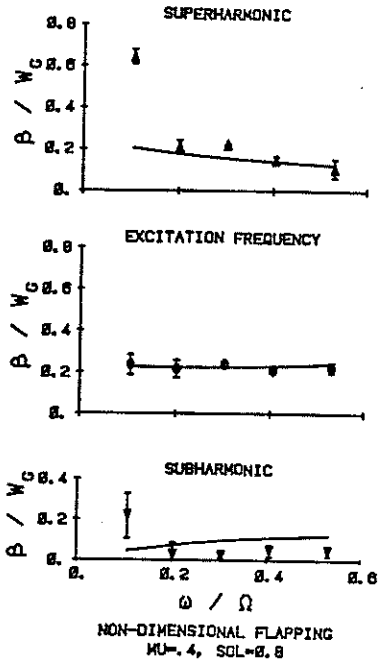

FIG. 11d (CONCLUDED)

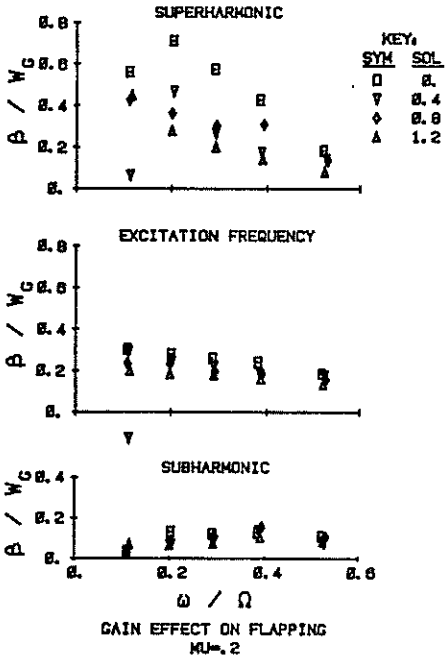

FIG. 12a EFFECT OF FEEDBACK GAIN ON FLAP RESPONSE TO GUST

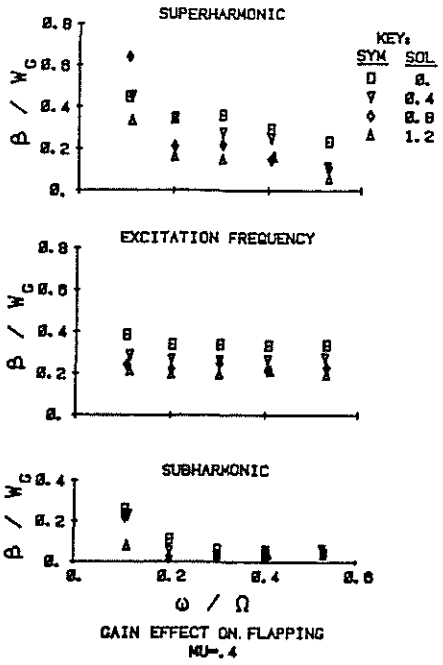

FIG. 12b (CONCLUDED)

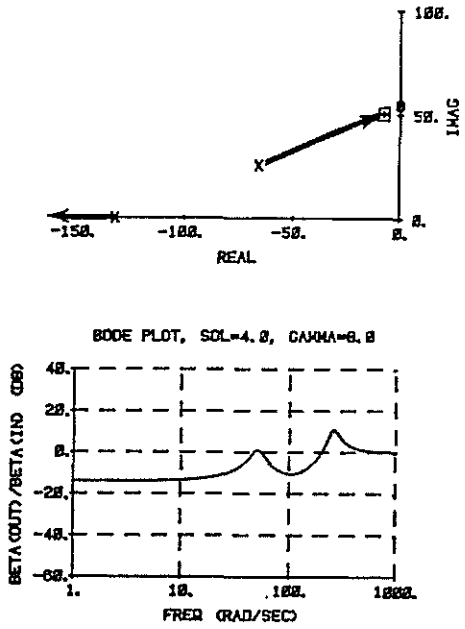

FIG. 13 FULL-SIZE COUPLED BLADE, ACCELEROMETER, AND MEDIUM-GAIN SERVO DESIGN

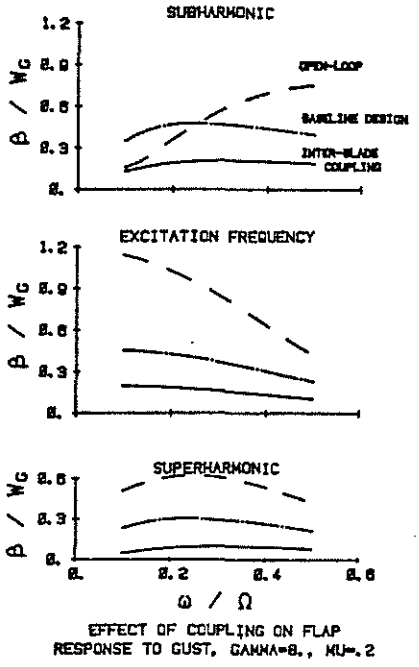

FIG. 14a FULL-SIZE COUPLED FLAP RESPONSE TO GUST

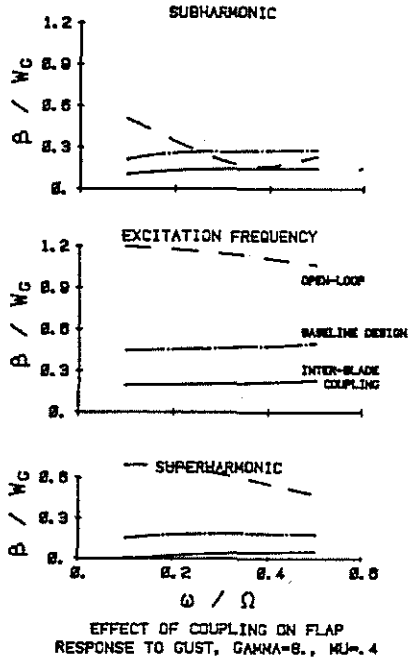

FIG. 14b (CONCLUDED)